Construction and Building Materials 290 (2021) 123251

Contents lists available at ScienceDirect

Construction and Building Materials

journal homepage: www.elsevier.com/locate/conbuildmat

Almond-shell biomass ash (ABA): A greener alternative to the use of commercial alkaline reagents in alkali-activated cement

Lourdes Soriano [a], Alba Font [a], Mauro M. Tashima [b], José Monzó [a], Maria Victoria Borrachero [a], Thaís Bonifácio [a], Jordi Payá [a,*]

[a] ICITECH – GIQUIMA Group – Grupo de Investigación en Química de los Materiales de Construcción, Instituto de Ciencia y Tecnología del Hormigón, Universitat Politècnica de Valencia, Valencia, Spain
[b] Universidade Estadual Paulista (UNESP), Faculdade de Engenharia de Ilha Solteira, MAC – Grupo de Pesquisa em Materiais Alternativos de Construção, Ilha Solteira, SP, Brazil

HIGHLIGHTS

- Almond-shell biomass ash (ABA) was used as an activator in alkali-activated cement.
- Blast furnace slag (BFS) was mixed with ABA to prepare the binder.
- Potassium salts in ABA promoted the hydraulicity of BFS to produce C(K)-A-S-H gel.
- Better compressive strength for ABA/BFS was obtained compared to KOH-activated BFS.
- Very low CO_2 emissions (50–60 $kgCO_2eq/m^3$ for ABA/BFS mortar) were calculated.

ARTICLE INFO

Article history:
Received 1 September 2020
Received in revised form 4 March 2021
Accepted 4 April 2021
Available online 17 April 2021

Keywords:
Almond-shell biomass ash
Blast furnace slag
Eco-friendly material
Waste valorisation
Alkali activated materials

ABSTRACT

The use of almond-shell biomass ash (ABA) as an alternative component to the commercial reagents used in the activation of blast furnace slag (BFS) systems is investigated. The presence in its chemical composition of a high content of K_2O indicates that it can alkalinize the medium. 100% waste-based mixtures ABA/BFS were studied by micro- and macrostructural tests. A compressive strength of 44 MPa was achieved by the mortar with 25% ABA addition cured for 7 days at 65 °C. The microstructural analysis showed the formation of slightly different C(K)-A-S-H gels to those formed when using KOH. The use of ABA in BFS mortars is shown as a greener alternative for construction materials because the replacement of synthetic chemical reagents that produced around a 75–80% of reduction in the values of $kgCO_2eq/m^3$ material.

1. Introduction

The alkali activated materials (AAMs) and geopolymers play an important role in the construction industry's sustainability. In many cases their production reduces CO_2 emissions compared to the ordinary Portland cement (OPC) production and the resulting materials (AAMs and geopolymers) that present good mechanical and durability properties [1]. The alkaline reaction is the result of mixing mainly amorphous silica, alumina and calcium-based precursor with high alkaline solution (alkali silicate/hydroxide). The precursor can be a natural or a waste material, such as metakaolin, fly ash, blast furnace slag, etc.[2].

The blast furnace slag (BFS) is one of the most widely used precursors in alkaline activation and fulfils the model proposed for materials rich in $CaO\text{-}SiO_2\text{-}Al_2O_3$ [2,3]. Their reactivity depends on their composition and the vitreous structure. One of the main advantages is that using highly concentrated alkaline solutions is not necessary. Furthermore, to obtain a stable BFS-based AAM matrix, curing can occur at both room and high temperatures [4–6].

Nowadays, one of the goals in the AAM investigations is the complete replace commercial reagents with waste materials to prepare the alkaline activating solution. Some research works have focused on studying residues from different sources: Jamieson et al. used Bayer liquor to produce geopolymers with two types of fly ash (FA) [7]. They demonstrated the possibility of obtaining mortars with compressive strengths of 20 and 40 MPa with the two types of FA using a 5% of hydrated lime and curing for 7 days at room temperature. Fernández-Jiménez et al employed aluminum industry waste (alkali solution discarded from washing aluminum casting molds) to prepare mixtures with FA [8]. The mortars fabricated with this waste achieved values around

* Corresponding author.
E-mail address: jjpaya@cst.upv.es (J. Payá).

https://doi.org/10.1016/j.conbuildmat.2021.123251
0950-0618/

16 MPa of compressive strength by a curing method that lasted 20 h at 85 °C and 28 days in a climatic chamber. These obtained values were very similar to the mortars activated with 8 M of NaOH.

The biomass is a high yield combustible capable of frequently covering the same needs as fossil fuels. Furthermore, the biomass is generally less expensive than natural gas or fuel. It can even have a zero cost if energy is required in the same factory that produces biomass waste.

The biomass ashes (BA) are the resulting solid by-products from the complete or incomplete combustion process. There are two types of such by-products: the biomass bottom ash or slag (BBA); and the biomass fly ash (BFA). Normally, the industrial combustion or gasification installations work within a burning biomass range of between 800 and 1600 °C.

In the last years, the use of BA with high SiO_2 contents to produce alternative activators has been studied. The rice husk ash (RHA) and sugar cane straw ash (SCSA) are suitable for its employment replacing commercial waterglass in the alkaline activating solution [9,10]. These alternative systems have been demonstrated the reduction in the carbon footprint up to 50% compared to conventional AAM systems with commercial reagents [11].

The use of potassium-rich ashes to prepare the alkaline reagent is a new challenge for the science community. Peys et al. [12] studied ashes from oak and beech, maize and cotton, which were combined with metakaolin (MK). In a preliminary phase, the best compressive strength result was obtained by the mixture with maize cob ashes, obtaining about 30 MPa after 2 days of curing at 80 °C and 5 days at room temperature. These authors proposed optimizing the curing process by curing at 20 °C during 24 h, followed by oven curing for 48 h at 80 °C. Under these conditions, the samples achieved a compressive strength of 40 MPa.

The use of olive stone biomass ash (OBA) has been studied in AAM since 2017. The role of OBA was analyzed in mixtures with BFS and FA as precursors [13–16]. In the first published paper, Font et al. [13] compared the behavior of the mixtures activated with KOH 4 M and 18.8% of OBA addition in the mixtures with BFS cured at 65 °C during 7 days. The mortars activated with OBA had a compressive strength of 30.0 MPa versus 18.8 MPa obtained for the mortar with KOH.

Alonso et al. [15] studied two types of olive biomass residues, the olive biomass fly ash (OBFA) and bottom ash (OBBA). In pastes with BFS used as a precursor, the samples with OBFA achieved higher strength than the pastes with OBBA by yielding about 33 MPa after curing 28 days at 45 °C while the paste with OBBA presented 18 MPa for the same curing conditions. In the pastes in which FA was used as a precursor, the use of OBA was not feasible because this precursor needs a higher pH to be activated. The radiological and leaching studies confirmed the compliance with the standards required by European legislation.

The OBA was combined with RHA to prepare ternary alkali activated materials and achieved compressive strength of 46 MPa when the mortar was cured at room temperature for 28 days [16]. The reaction between OBA and RHA led to the formation of an alternative potassium silicate, which enhanced the reaction toward BFS compared to using only OBA as the alkaline activator.

Lin et al. [17] proposed using wood biomass fly ash (WBA) as an alkaline activator in mixtures with coal fly ash (FA). These authors studied mixtures with 15% FA and 85% WBA. The principal oxides with this ash were CaO (38.1%) and K_2O (12.2%). These authors studied the influence of different parameters: water/ash ratio, curing method and activator type (water or Na_2SiO_3 solution). Their paper analyzed different physico-chemical properties by several techniques, such as SEM or XRD analysis. However, the most interesting study was the leaching test. With this test, the research work concluded that good performance can be achieved without using Na_2SiO_3.

Vassilev et al. [18] proposed classifying BA depending on the main oxide contents: S, K, C and CK type. These authors found references about 80 biomass varieties and the data for almond-shell biomass ash presented high content of potassium (K_2O = 53.48%). This ash belongs to K type. Some other ashes from husks/shells/kernels/pits belong to this type, like coffee, sunflower and cotton husks, hazelnut and walnut shells, palm kernel and plum pit.

The USA is the world's leader in almond production, with a market share of approximately 80%. Spain is the third producer with a market share of 5% [19]. In 2019/2020, the world's almond production was around 1.363,7 million tons [20]. The shell represents 3/4 of an almond [21]. The almond shell has 28.8% lignin, 56.1% polysaccharides (cellulose and hemicellulose), 5.7% total extractives and 0.7% ash [22].

The almond shell (AS) is considered fruit biomass, more specifically fruit shell [23]. Some studies have examined the feasibility of using AS as biomass [24–27]. Pinna-Hernández et al. [24] studied five different biomass samples from Almería (Spain) to conclude that the best biomass was the AS for its high calorie value (19,288 kJ/kg) and low sulfur and chlorine contents.

Similar conclusions were drawn by García et al. [25]. These authors studied 13 samples as possible biomass fuels in the combustion process. They concluded that AS and olive stone (OS) were the best options because they presented good parameters like heating value and bulk density, low emissions and competitive costs.

Aktas et al. [26] characterized almond waste from different locations in California. They concluded that the high potassium content in AS and hull (18–36% wt%) allow the corresponding ashes to be considered to offer a high-potential application as an electrolyte or fertilizer.

To investigate the potential use of ABA as an alkaline activator, this study characterized ABA from an industrial boiler and analyzed its use in mixtures with BFS to prepare 100% waste-based AAMs. Two paths were followed: replacing BFS (5–35% in weight) and addition in relation to a constant amount of BFS (5–25% in weight). A comparison to commercial reagents was made to assess the feasibility of employing ABA as an alternative component in AAMs.

The novelty of this research is focused on the complete characterization of ABA, the design of new dosages for mortars to evaluate the effectiveness of this new activator and the achievement of new binders with a low carbon footprint.

2. Materials and methods

2.1. Materials

The almond-shell biomass ash (ABA) was supplied by Borges Agricultural & Industrial Nuts (Altura, Spain). The sample taken from the industrial boiler was sieved to remove particles larger than 5 mm in size. The sieved sample was milled in a ball mill for 10 min (ball mill model Speedy of Nannetti). Blast furnace slag (BFS) was supplied by Cementval (Puerto de Sagunto, Spain). BFS was ground in a ball mill for 30 min to obtain an adequate particle mean diameter of 26 μm. Commercial KOH pellets were supplied by Panreac S.A (85% purity).

2.2. Methods

For the mechanical tests, mortars were prepared with different BFS/ABA mass ratios. Two control mortars with the commercial

reagent (KOH) were also prepared. The ABA-containing mortars included two mixture types: the replacement (Rp) and addition (Ad) series. The Rp series were prepared by substituting BFS by ABA. The Ad series were prepared by maintaining the same amount of BFS as for the control mortars, and adding ABA in increasing percentages in relation to BFS. The Rp series had five mixtures from 15% to 35% replacement (BFS with ABA). The Ad series had five mixtures from 5% to 25% of Ad (ABA in relation to the BFS weight).

The mortars of the Rp series were prepared at a water/solid ratio of 0.4 and a sand/solid ratio of 3. The solid in this series was the sum of BFS and ABA, and was always 450 g for each batch. The control mortars were prepared by activating BFS (as a precursor) with KOH dissolved in water (two different molalities, mol of KOH per kg of water, were used: 4 mol and 8 mol), with the same water/solid and sand/solid ratios as the Rp series. For the Ad series, these ratios were different for each addition percentage because the amount of sand and water was the same as in the control mortars (these quantities were set at 1350 g and 180 g, respectively, for each batch). The solid was the sum of BFS and ABA (values between 482.5 and 562.5 g). The doses of mortars are summarized in Table 1. For each ABA containing mortar, the BFS/ABA mass ratio was calculated.

The mortars were prepared and poured in prismatic molds ($4 \times 4 \times 16\ cm^3$). Specimens were cured for 3 and 7 days at 65 °C. Three values for flexural strength and six for compressive strength were calculated according to the conditions specified in UNE 196-1 [28].

The pastes used for the microstructural analysis were prepared at a water/solid ratio of 0.4 and were molded in a plastic container with a lid to avoid carbonation and water evaporation processes. The selected pastes were prepared for the microstructural analysis: 4 m KOH, 8 m KOH and Rp20. The analysis performed for 3 and 7 curing days at 65 °C were: a) XRD analysis (carried out by Brucker equipment); b) thermogravimetric analysis (TGA) (by TGA850 Mettler Toledo equipment); c) field emission scanning electron microscopy (FESEM) and energy dispersive X-ray spectroscopy (EDS) (using an ULTRA 33-Zeiss equipment).

The X-ray diffraction (XRD) analysis was performed by Brucker AXS D8 Advance (Billerica MA). Patterns were taken from 10° to 70° 2θ Bragg angle, with Cu Kα radiation at 20 mA and 40 kV. The time accumulation was 2 s with a 0.02°-angle step. The TGA analyses were carried out within a temperature range of 35–600 °C using aluminum crucibles (sealed with a pin holed lid) at a heating rate of 10 °C/min in an N2 atmosphere (flow gas of 75 mL/min). The samples for the FESEM analysis were covered with carbon and analyzed at 2 kV to obtain images. For the EDS analysis, voltage was 20 kV. The chemical compositions of ABA and BFS were measured by X-ray fluorescence (XRF) (Philips Magix Pro spectrometer).

The 100-year Global Warming Potential time horizon (GWP100) was calculated according to the Standard ISO 14,040 and the Intergovernmental Panel on the Climate Change 2006 (IPCC) Guidelines for National Greenhouse Gas Inventories specifications [29]. The total $kgCO_2eq/m^3$ of the manufactured mortar was obtained as the sum of the following unitary equations for each considered raw material or procedure: Eq. (1):

$$\mathbf{E_i} = \mathbf{A_i} \cdot \mathbf{EF_i} \quad (1)$$

where:

$\mathbf{E_i}$ = $kgCO_2eq/m^3$ of the manufactured mortar for each raw material or procedure "i"; $\mathbf{A_i}$ = amount of raw material or procedure "i" to prepare 1 m^3 of mortar; and $\mathbf{EF_i}$ = emission factor-associated (CO_2 emission) per unit of each raw material or procedure "i".

A "gate-to-gate" modality of the Life Cycle Assessment (LCA) was carried out, in which the GWP100 associated with obtaining raw materials (AAM components: precursor, activator, water and sand) and its conditioning procedure (milling treatment) were considered. The mixing, compacting and curing procedures were not taken into account in the calculations because they were exactly the same activities for all the compared mortars. The Ecoinvent 3.3 inventory and the national energy mix (2018) were the datasets employed for the emission factors associated with CO_2 emissions (EFi). For the grinding process of BFS and ABA, the following experimental conditions were considered: a) mill power: 0.3 kW; b) for BFS milling: 0.45 kg of slag ground for 30 min; c) for ABA milling: 0.25 kg of ash ground for 10 min. The impact factor was taken to be 0.272 $kgCO_2/kWh$ [30].

3. Results and discussion

3.1. Physico-chemical characterization of ABA

The ABA showed moderate alkalinity: the ash (4 g) was stirred for 4 h in deionized water (100 mL). The pH and electrical conductivity values were 10.54 and 8.98 mS/cm, respectively. The pH value was lower than that obtained for K_2CO_3 (4 g in 100 mL), which suggests that alkalinity was similar. It has been reported

Table 1
Mortar doses for the control, replacement (Rp) and addition (Ad) series.

Mixture	BFS (g)	Potassium source			H_2O (g)	Sand (g)
		Type	Quantity (g)	BFS/ABA mass ratio		
		CONTROLS				
4 mol	450.0	KOH	47.4*		180.0	1350
8 mol	450.0	KOH	94.9*			
		REPLACEMENT SERIES (Rp)				
Rp15	382.5	ABA	67.5	5.7	180.0	1350
Rp20	360.0	ABA	90.0	4.0		
Rp25	337.5	ABA	112.5	3.0		
Rp30	315.0	ABA	135.0	2.3		
Rp35	292.5	ABA	157.5	1.9		
		ADDITION SERIES (Ad)				
Ad5	450.0	ABA	22.5	20.0	180.0	1350
Ad10	450.0	ABA	45.0	10.0		
Ad15	450.0	ABA	67.5	6.7		
Ad20	450.0	ABA	90.0	5.0		
Ad25	450.0	ABA	112.5	4.0		

*This quantity corresponds to the amount of commercial reagent (85% purity).

Table 2
Main granulometric parameters of ABA and BFS.

	d mean (μm)	d (0.1) (μm)	d (0.5) (μm)	d (0.9) (μm)
ABA	18.8	2.3	12.3	45.2
BFS	26.0	2.8	20.6	66.2

that some BAs (e.g. wood ash) presented solubilization of some mineral phase, which alkalinizes soil and increases pH [31].

Table 2 summarizes the samples' main size particle parameters after the milling process. Particle size distribution was measured by laser diffraction in a Mastersizer 2000 (Malvern Instruments) with water as the dispersant liquid. After only 10 min of grinding, ABA had an average particle diameter of less than 20 μm.

The chemical compositions of ABA and BFS are summarized in Table 3.

The major oxides present in ABA were the K_2O and CaO (46.98% and 18.73%, respectively), which coincided with previously reported data [32]. The percentage of K_2O was higher than for the previously studied OBA [13,15]. The high value of this oxide indicated ABA's positive potential behavior as an alkaline activator.

The LOI of ABA was very high (28%), probably due to: a) poor combustion in the boiler which could leave some material unburned; b) presence of carbonates (calcium carbonate and double carbonates of potassium and calcium). The LOI was measured in a muffle furnace from 700 °C because some material sinters at higher temperatures due to the presence of potassium salts. ABA was analyzed by the TGA by heating the sample within the 35–1000 °C range. Total mass loss was 33.39%, which corroborated the presence of carbonates and unburned particles. In order to clarify the origin of the high LOI value, an additional test was performed. The amount of carbonates was determined by means the reaction of ABA with hydrochloric acid and measuring the volume of CO_2 gas evolved in the process. The mass percentage of CO_2 evolved was 31.5%, this value is similar to the LOI test, suggesting that the main decomposition was related to decarbonatation of some compounds in the ash.

The Fig. 1 shows the XRD patterns of ABA and BFS. A key letter represents the mineral phases presented in ABA and BFS. Table 4 summarizes the mineral phases with their chemical formula and the PDF card.

The XRD pattern of BFS showed that this material was mainly amorphous with some small peaks related to certain crystalline phases (calcite and quartz).

The main crystalline phases of ABA were calcite, fairchildite and bütschilite. Minor phases were detected: portlandite, arkanite, anhydrite, gypsum, kovdorskite. The ABA also presented an amorphous fraction, as seen in the deviation of the baseline between 2θ values of 20° and 35°.

The morphology of the original and ground ABA particles is depicted in Figs. 2 and 3, respectively. The original ABA had irregular particles of different shapes and sizes (see Fig. 2a and c). Fig. 2b shows that many amorphous particles are covered by very small crystals (plates and prisms). These crystalline particles were probably produced after firing the almond shell and the subsequent carbonation: these were the K-Ca carbonates identified by the XRD analysis. In the same way, some unburned particles are clearly identified in the sample (Fig. 2d). For ground ABA, particles were smaller, but some large particles remained after grinding (Fig. 3a and c). The unburned particles were also observed (Fig. 3b) and many well-shaped crystals were not found because of the grinding process (Fig. 3d). Some particles are present as partially broken crystals.

In order to verify the carbonates formation in ABA, a sample of almond shell (Fig. 4) was calcined at 600 °C for 1 h in a furnace. After calcination process, this sample was collected and stored in a hermetic vessel to avoid carbonation. As can be observed in Fig. 5, the resulting ash did not present the crystal-shaped particles, typical of carbonates.

3.2. Mechanical properties of mortars

The effect of ABA as an alternative activator was assessed by studying the flexural (F_s) and compressive (C_s) strengths after 3 and 7 curing days at 65 °C. The results are summarized in Table 5.

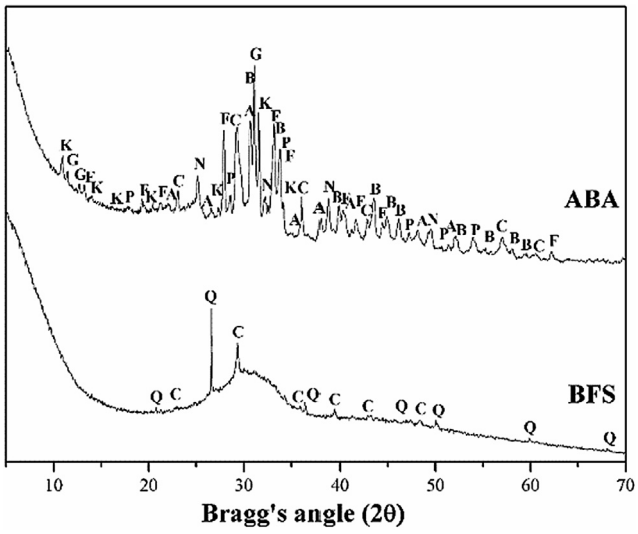

Fig. 1. The X-ray diffraction patterns of ABA and BFS.

Table 4
XRD characterization: keys, name of minerals, PDF card and chemical formula of the phases present in ABA and BFS.

KEY	MINERAL PHASE	CHEMICAL FORMULA	PDFcard
C	Calcite	$CaCO_3$	050,586
Q	Quartz	SiO_2	331,161
A	Arkanite	K_2SO_4	050,613
P	Portlandite	$Ca(OH)_2$	040,733
F	Fairchildite	$K_2Ca(CO_3)_2$	211,287
B	Bütschilite	$K_2Ca(CO_3)_2$	250,626
N	Anhydrite	$CaSO_4$	271,496
K	Kovdorskite	$Mg_2(PO_4)(OH).3H_2O$	330,861
G	Gypsum	$CaSO_4{\cdot}2H_2O$	330,311

Table 3
Chemical composition for ABA and BFS.

	Oxide composition (%)										
	SiO_2	CaO	Al_2O_3	Fe_2O_3	Na_2O	MgO	K_2O	P_2O_5	SO_3	others	LOI*
ABA	0.64	18.73	0.19	0.47	0.37	1.68	46.98	1.74	0.68	0.52	28.00
BFS	30.53	40.15	10.55	1.29	0.87	7.43	0.57	0.26	1.93	0.89	5.53

* Loss on ignition at 700 °C for 1 h.

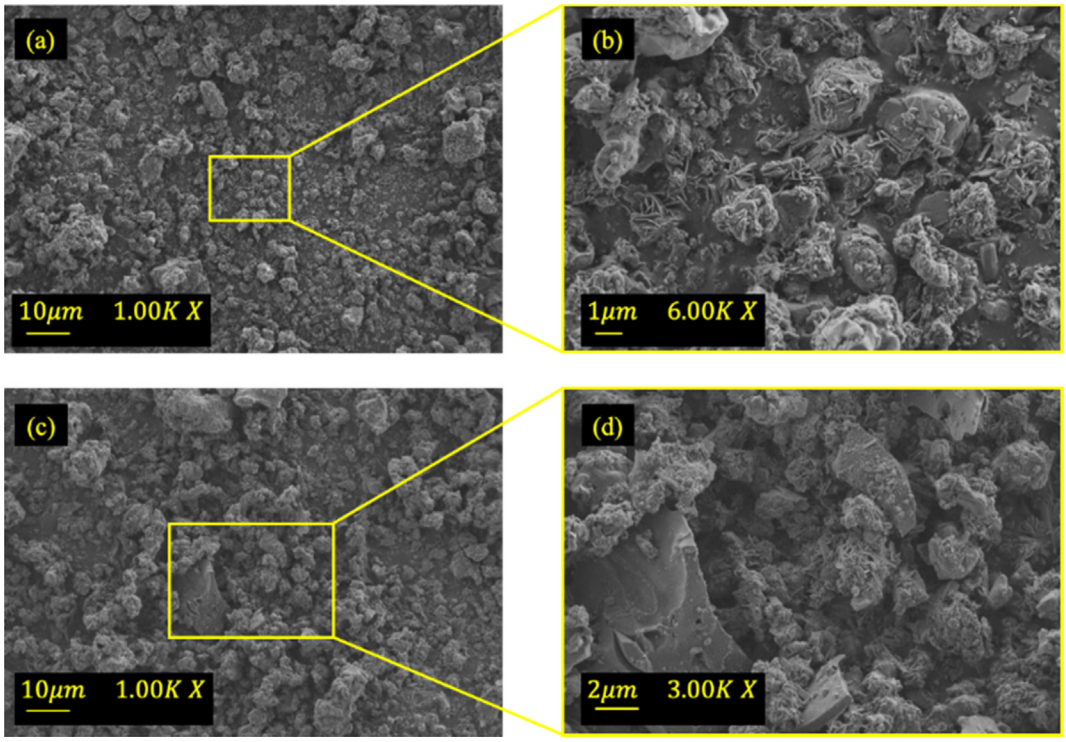

Fig. 2. FESEM micrographs of the original ABA: a) general view; b) detailed view of crystalline particles; c) general view with a large unburned particle; d) detailed view of an unburned particle (left bottom corner).

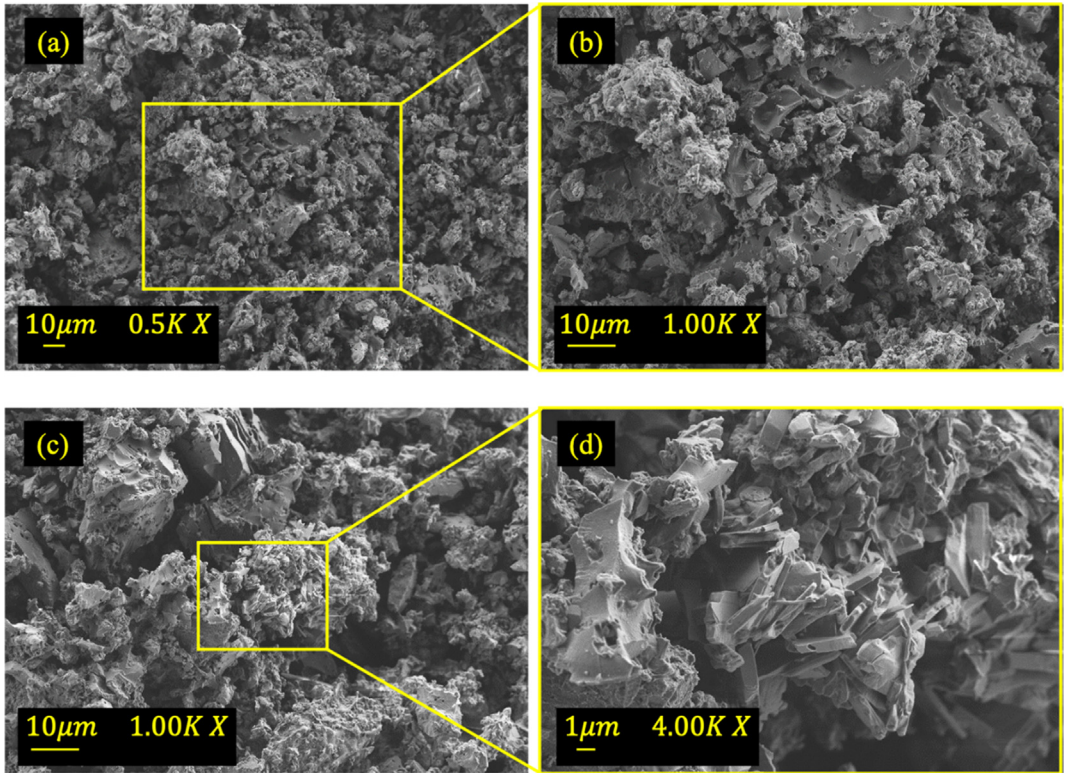

Fig. 3. FESEM micrographs of ground ABA: a) general view; b) detail of an unburned particle (center of the micrograph); c) general view; d) detailed view of broken crystals.

The F_s values of the control mortars were between 3.3 and 5.1 MPa. Hardly any differences were found between 3 and 7 curing days for the 4 mol control mortar (from 3.3 to 3.8 MPa), but the 8 mol control significantly increased from 3.8 to 5.1 MPa. The highest C_s value was 26.6 MPa for the 8 mol KOH activated mortar after 7 curing days at 65 °C. For this reason, in the following discussions the 8 mol control mortar was taken into account for the comparisons to the ABA-containing mortars.

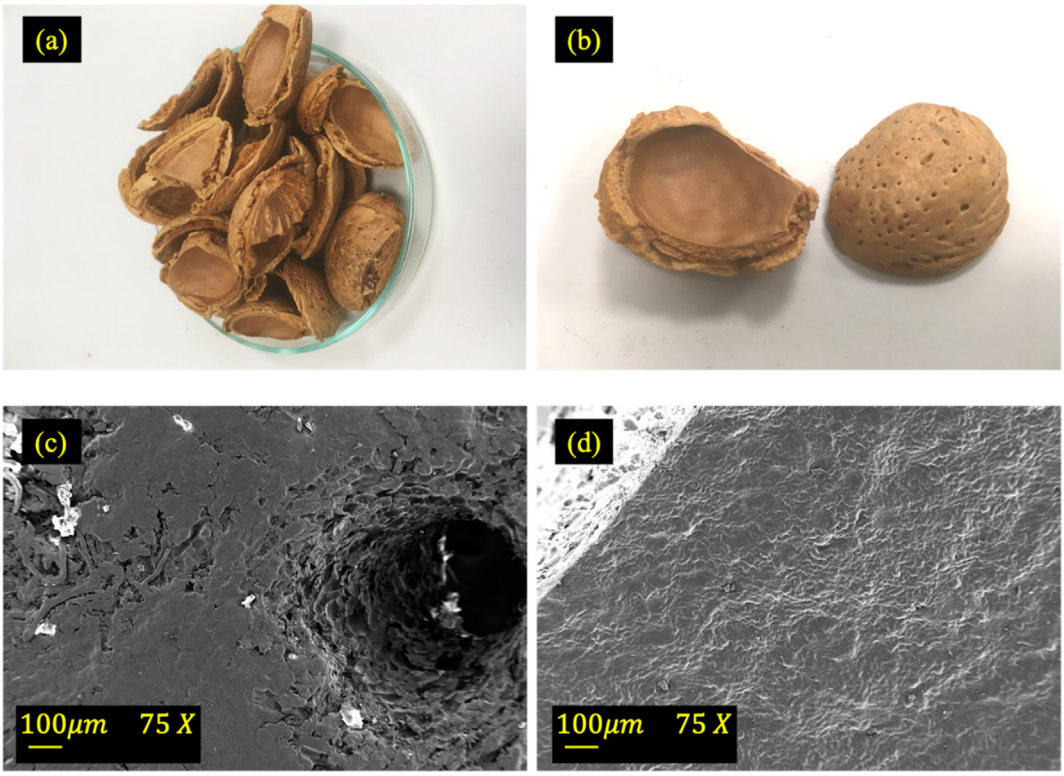

Fig. 4. Images of almond shells: a) general view; b) outer (down) and inner (up) parts of the shell; c) FESEM micrograph of outer part; d) FESEM micrograph of inner part.

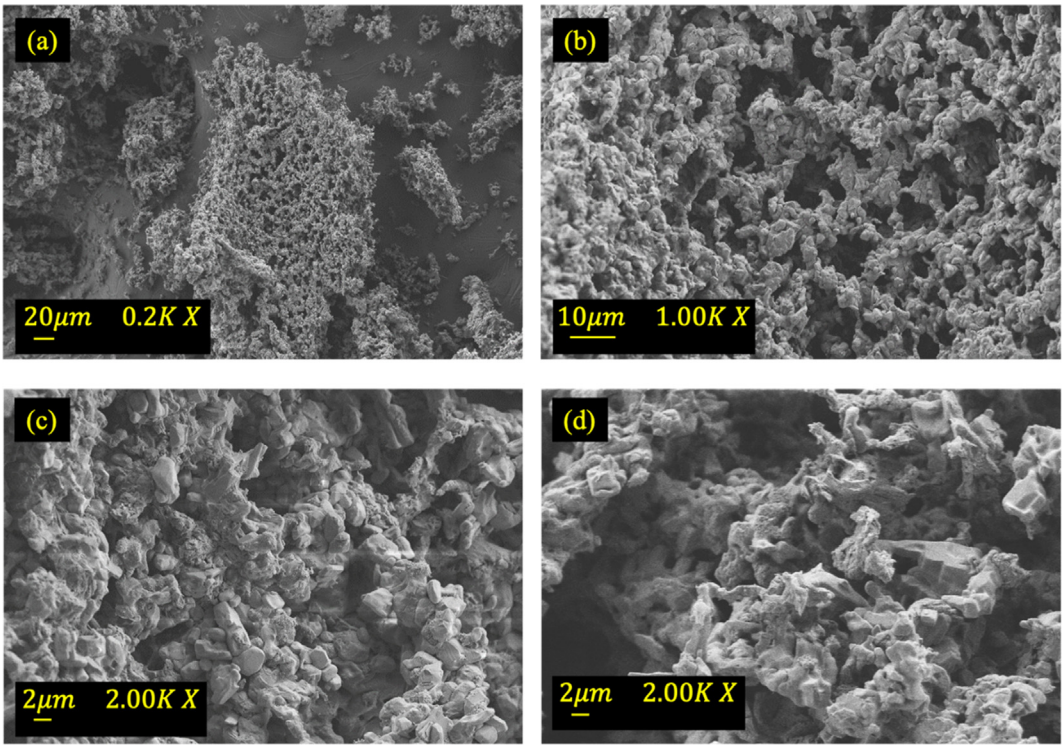

Fig. 5. FESEM micrographs of ashes obtained from almond shell calcined in an oven at 600 °C for 1 h (after, stored in a hermetic vessel to avoid further carbonation): a), ×200 b) ×1000 c) ×2000; d) ×2000.

For the Rp series, the F_s values were similar or higher than those obtained for the 8 mol control mortar after 3 and 7 curing days, except for the Rp35 sample, with 4.3 MPa after 7 curing days (significantly lower than 5.1 MPa for the 8 m KOH sample). The general behavior of the Rp series was significantly better than the 8 mol mortars for both curing ages. The C_s values significantly

Table 5
Values of the flexural and compressive strengths of the mortars cured at 65 °C for 3 and 7 days.

Mortar	3 days		7 days	
	F_s (MPa)	C_s(MPa)	F_s(MPa)	C_s (MPa)
CONTROL				
4 mol	3.3 ± 0.2	13.7 ± 0.7	3.8 ± 0.3	20.9 ± 0.5
8 mol	3.8 ± 0.1	19.7 ± 0.6	5.1 ± 0.2	26.6 ± 1.0
	REPLACEMENT SERIES (Rp)			
Rp15	3.8 ± 0.5	17.9 ± 0.5	5.1 ± 0.2	30.7 ± 1.0
Rp20	3.7 ± 0.2	21.7 ± 2.5	5.2 ± 0.2	34.0 ± 0.9
Rp25	4.5 ± 0.4	23.9 ± 1.2	5.3 ± 0.4	35.2 ± 0.8
Rp30	3.6 ± 0.1	25.1 ± 0.6	5.2 ± 0.3	33.1 ± 0.7
Rp35	3.7 ± 0.5	22.3 ± 0.7	4.3 ± 0.8	26.2 ± 0.5
	ADDITION SERIES (Ad)			
Ad5	3.3 ± 0.3	13.6 ± 1.3	3.4 ± 0.2	14.4 ± 0.9
Ad10	4.1 ± 0.3	22.3 ± 0.8	4.7 ± 0.8	24.0 ± 0.5
Ad15	6.0 ± 0.5	29.9 ± 1.0	5.6 ± 0.1	34.3 ± 0.6
Ad20	6.1 ± 0.4	33.8 ± 1.7	6.3 ± 0.6	42.4 ± 1.0
Ad25	5.2 ± 0.4	31.7 ± 0.3	5.2 ± 0.3	45.2 ± 0.5

increased from 3 to 7 curing days (increase of 8–13 MPa from samples Rp15 to Rp30). These results suggested that BFS alkaline activation by ABA replacement was successful: dissolution of one part of ABA was achieved, and the dissolved alkaline and hydroxyl ions promoted BFS hydraulicity.

The BFS/ABA mass ratio in the Rp series varied from 5.7 (Rp15) to 1.9 (Rp35). The relation between BFS/ABA ratio and C_s is shown in Fig. 6. The fitting equation Eq (2)[33] was:

$$\boldsymbol{C_s} = 41.73 - (1.93 * \boldsymbol{x}) - (1627 * 0.075^{\boldsymbol{x}}) \mathrm{R-squared} = 0.999 \quad (2)$$

where: x is the BFS/ABA mass ratio.

The optimum BFS/ABA ratio was 2.97 (maximum of the curve, 35.2 MPa), which means that to obtain the best results, the replacement percentage would have to be 25.19%. When the BFS/ABA ratio was very low (e.g. 1.9 for Rp35), the reduction in BFS content produced fewer cementing hydrates, besides the high alkalinity of the medium (achieved by the high ABA content). Moreover, for this dose, the workability of the fresh mixture was poor and this would, consequently, promote a less compacted matrix.

For the Ad series, the F_s values were generally higher than or similar to the 8 m control. The lowest F_s values were obtained for the Ad5 sample: in this case, the small amount of ABA did not allow enough alkalinity to properly allow a good hydraulic reaction of BFS. With an increasing ABA content, F_s increased, except for Ad25-7 days: in this case, probably the low workability of the fresh mixture produced a relatively low strength when the mortar was cured (5.2 MPa, 7 days 65 °C). In C_s parameter terms, we found that lower BFS/ABA ratios enhanced developing the cementing matrix. In this case, the lowest C_s values were found for BFS/ABA ratios of 20 (Ad5) and 10 (Ad10), whereas good strength development was observed for the other mortars (BFS/ABA ratios of 6.7, 5 and 4 for Ad15, Ad20 and Ad25, respectively). We can see that these C_s values were higher than those found for the optimum ones in the Rp series (35.2 MPa). For the Ad series, the water/solid ratio lowered when ABA increased and, consequently, the matrix was more compacted. In this case, the fitting equation for the relation between the BFS/ABA mass ratio (x) and compressive strength (C_s) for 7 curing days at 65 °C was (Eq. (3)):

$$\boldsymbol{C_s} = 11.46 + (65.73 * 0.85^{\boldsymbol{x}}) \mathrm{R-squared} = 0.989 \quad (3)$$

Fig. 7 depicts the above-mentioned curve and the experimental data. This curve shows the notable increase in C_s with ABA addition. For BFS/ABA values below 4, the preparation of mortars was impossible given their very dry consistency under fresh conditions. Therefore, this curve was valid only for the BFS/ABA ratio range from 4 to 20. In the same graph, the fitted curve for the Rp series are compared. We can see the greater strength for the Ad series

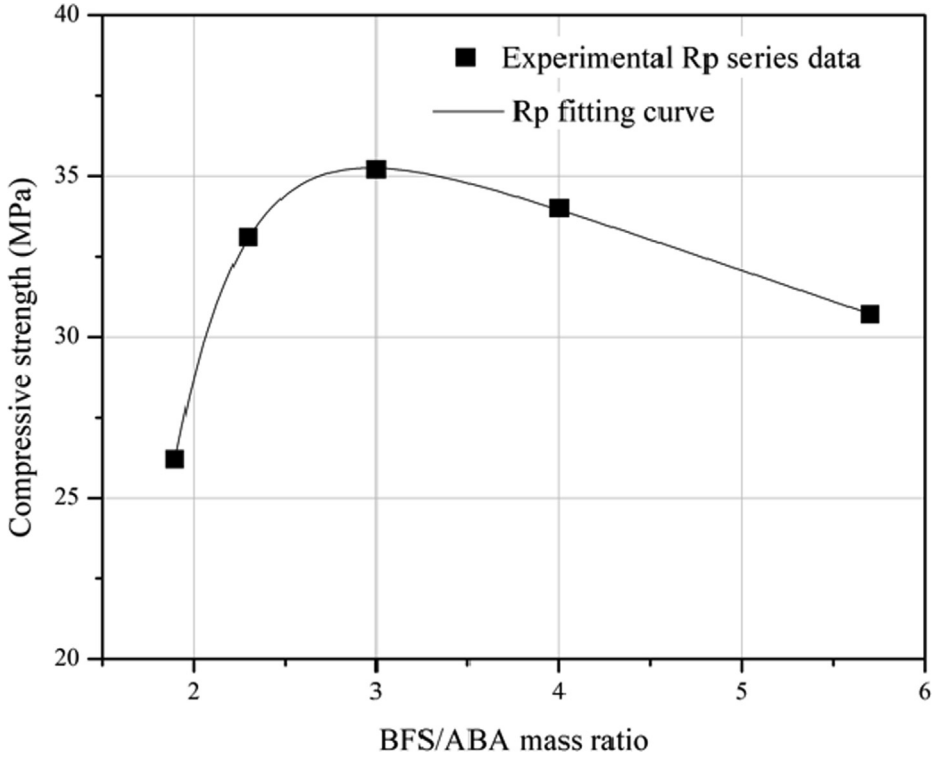

Fig. 6. Relation between compressive strength (C_s, 7 days 65 °C curing) and the BFS/ABA mass ratio in the replacement (Rp) series.

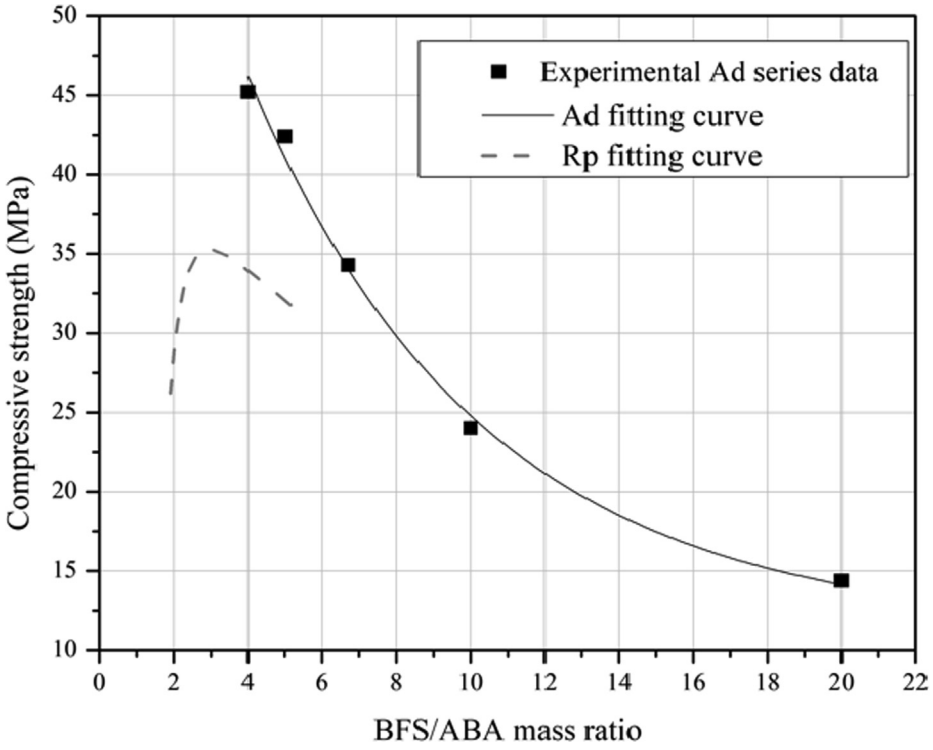

Fig. 7. Relationship between compressive strength (C_s, 7 days 65 °C curing) and the BFS/ABA ratio in the addition (Ad) series (the fitting for the Rp series is also presented as a dashed line).

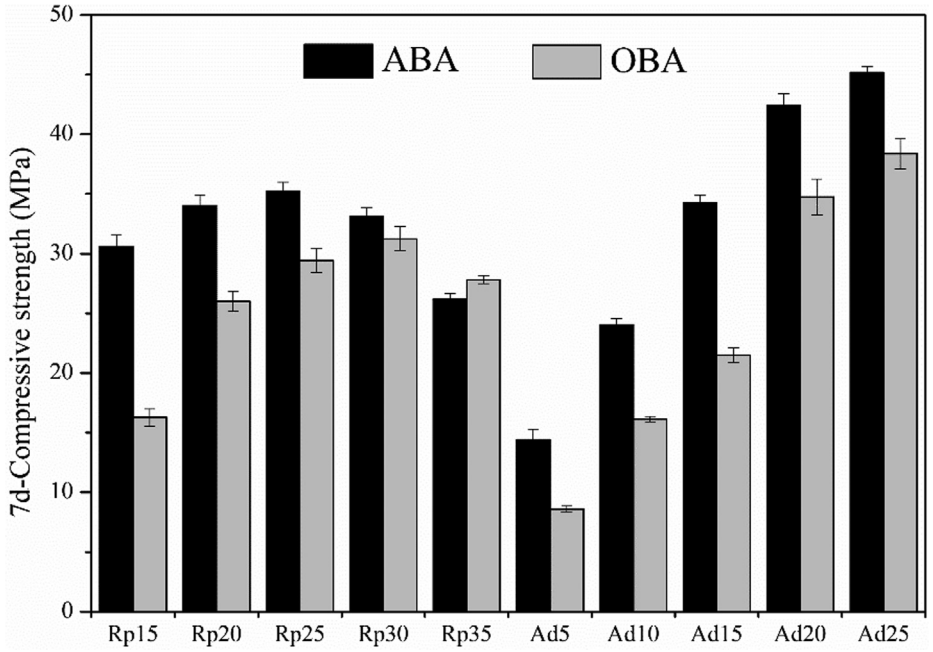

Fig. 8. Values of the compressive strength (MPa) of the mortars with ABA and OBA cured at 65 °C for 7 days: left, replacement series (Rp, 15–35% replacement of BFS with ash); right, addition series (Ad, 5–25% addition in relation to a constant mass of BFS).

mortars within the BFS/ABA common range compared to the Rp mortars (from ca. 4 to 6), which is due to the lower water/solid ratio for the Ad mortars.

In a previous paper [14], it was developed the study of the olive biomass ash (OBA) as source of potassium for alternative activator: this ash was tested in replacement and addition series in a similar experimental condition than ABA in the present research. Fig. 8 compares the compressive strength values obtained for the OBA- and ABA-containing mortars, which were prepared in the same component proportions and with the same precursor.

The C_s trends were similar for both ashes, is worth noting that ABA effectiveness was greater than OBA under the same conditions. OBA-mortar Rp15 had a compressive strength value of 16.3 MPa and the OBA-mortar Rp30 had one of 31.3 MPa. This last

value was similar to the values obtained in all the replacement percentages for the ABA-mortars. In the Ad series, the mortars with ABA achieved significantly higher compressive strengths than the OBA mortars; e.g., the ABA-mortar Ad25 had a compressive strength of 45.2 MPa, whereas the equivalent OBA-mortar obtained 38.4 MPa. The different behavior noted between both ashes was attributed to the different potassium percentages: 46.98% K_2O for ABA versus 32.26% for OBA [14], and to the presence of soluble salts [34], such as K-Ca carbonates (fairchildite and bütschilite). It is well-known that alkali carbonate is a good activating reagent for BFS [35,36].

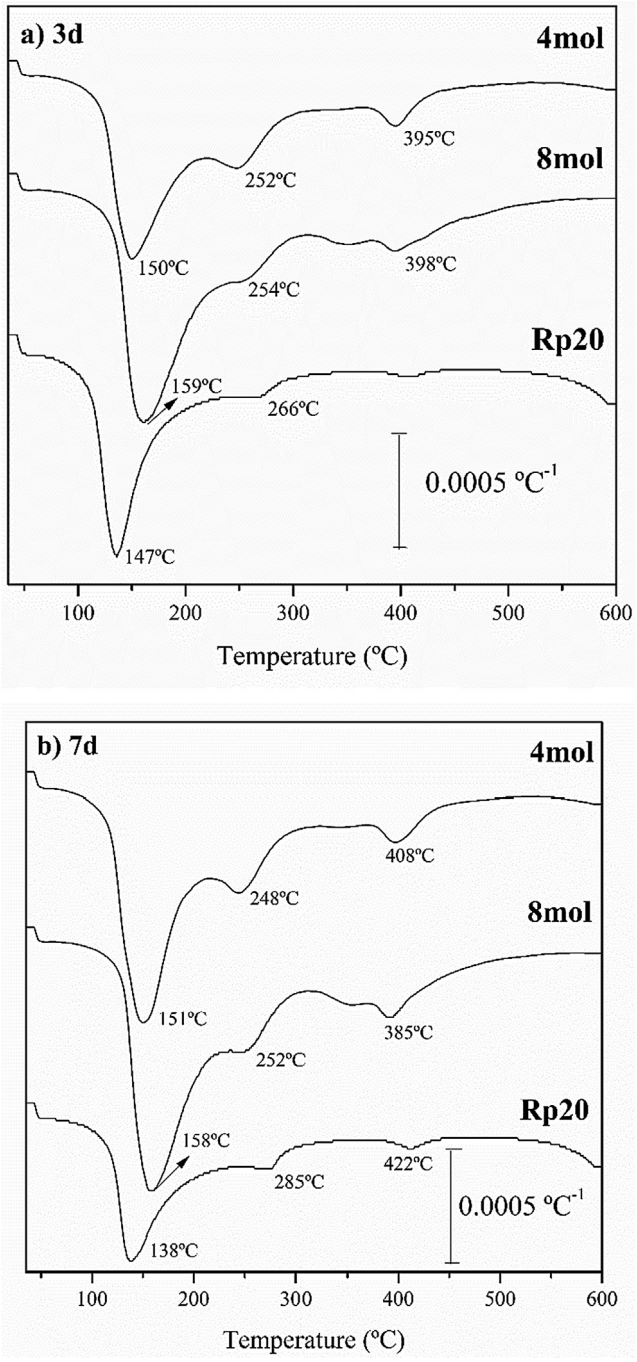

Fig. 9. DTG curves of pastes 4 mol and 8 mol KOH and the paste with 20% BFS replacement with ABA (Rp20) cured at 65 °C: a) 3 curing days; b) 7 curing days.

3.3. Pastes characterization

To compare the nature of hydration products when KOH and ABA were used as activating reagents, the control pastes 4 mol and 8 mol KOH and Rp20 pastes were characterized.

The TGA was performed for 3 and 7 curing days at 65 °C. Fig. 9 represents the DTG curves. As shown, three peaks were detected in the DTG curves. The largest peak was attributed to the water loss of C-S-H and C(K)-S-H [14]. The second peak appeared above 200 °C and was attributed to the mass loss of C-A-S-H and (C,K)-A-S-H products. Finally, the third peak around 400 °C was attributed to the presence of hydrotalcite; this compound had different peaks of mass loss but the other peaks overlapped with the previously described decomposition processes. The mass loss around 400 °C was attributed to the dehydroxylation and decomposition of the interlayer carbonate anion [37–39].

The temperatures of the first peak differed from the alkaline activator. The pastes with KOH presented a peak around 150–160 °C, while the pastes activated with ABA showed a peak at around 138 °C. This difference was attributed to a variation in the produced gels' chemical composition.

The peaks observed around 400 °C were attributed to hydrotalcite and were more pronounced in the pastes activated with KOH than in those activated with ABA.

As seen in Fig. 9, the DTG curves were similar for both curing days. After 7 days, peaks were more intense. This behavior indicates the evolution of the activating reaction of BFS, as corroborated by studying compressive strength development.

After 3 curing days, the total mass loss percentages (35–600 °C range) for pastes 4 mol, 8 mol and Rp20 were 10.5, 13.1 and 9.3%, respectively. After 7 days, the mass loss percentages were respectively 13.2, 15.4 and 9.4 for the same pastes. These results indicated that the amount of water combined in the pastes activated with a commercial reagent (KOH) was bigger than that in the paste activated with ABA. However, this difference in the amount and nature of hydration products had no negative effect on the compressive strength behavior of the ABA-containing system.

The X-ray diffraction patterns for the pastes cured at 7 days are depicted in Fig. 10. Table 6 summarizes the mineral phases present in pastes. Both pastes with KOH had very similar patterns with only a few differences related to the intensity of the diffraction

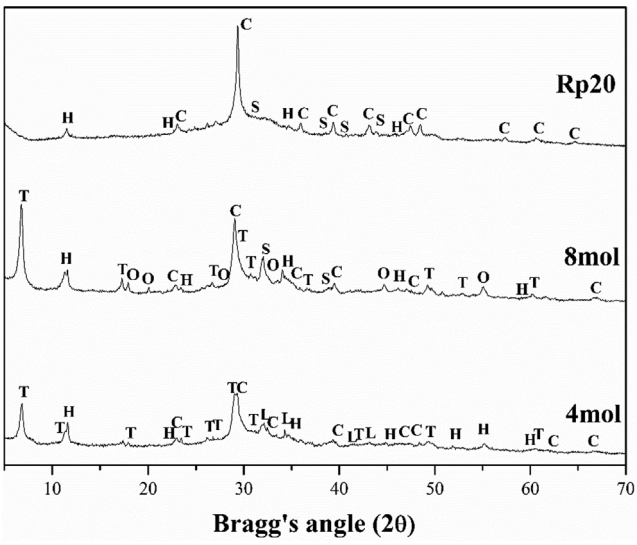

Fig. 10. X-ray diffraction patterns of the pastes cured at 65 °C for 7 days: 4 mol KOH; 8 mol KOH and Rp20 pastes (Key: C: calcite; H: hydrotalcite; L: larnite; O: katoite; S: hydrated potassium carbonate; T: tobermorite-14 Å).

Table 6
XRD characterization: name of minerals, PDF card of phases and chemical formula of the phases present in pastes.

T	Tobermorite-14 Å	$Ca_5Si_6O_{16}(OH)_2{\cdot}7H_2O$	060,005
L	Larnite	β-Ca_2SiO_4	330,302
H	Hydrotalcite	$Mg_6Al_2CO_3(OH)_{16}{\cdot}4H_2O$	140,191
C	Calcite	$CaCO_3$	050,586
S	Hydrated potassium carbonate	$K_2CO_3{\cdot}1.5H_2O$	110,655
O	Katoite	$Ca_3Al_2(SiO_4)(OH)_8$	380,368

peaks. Both pastes had signals that corresponded to the following mineral phases: hydrotalcite, calcite and tobermorite-14 Å [40]. Hydrotalcite was observed in the DTG study and was one of the typical alkaline activation products of BFS [13,41,42]. Calcite was a typical product of the original BFS. Tobermorite-14 Å was related to the hydrated phase identified in DTG (the first peak). Larnite was identified in paste 4 mol, while katoite was identified for paste 8 mol. Hydrated potassium carbonate was identified and the presence of this product was attributed to the carbonation process of KOH, both in paste 8 m [14].

In the Rp 20 paste, the main peak was attributed to the presence of calcite, and this phase was present in both ABA and BFS. The main crystalline product of the reaction was hydrotalcite. Tobermorite-14 Å s was absent in the Rp20 paste. Hydrated potassium carbonate was detected as a minor phase.

The significant differences in the XRD patterns of pastes was noteworthy, and was attributed to the difference in the nature of the alkaline source. With the KOH-activated pastes, the K_2O/BFS mass ratio was 0.075 and 0.150 for 4 mol and 8 mol, respectively. In both cases, the nature of the mineral phases identified by the

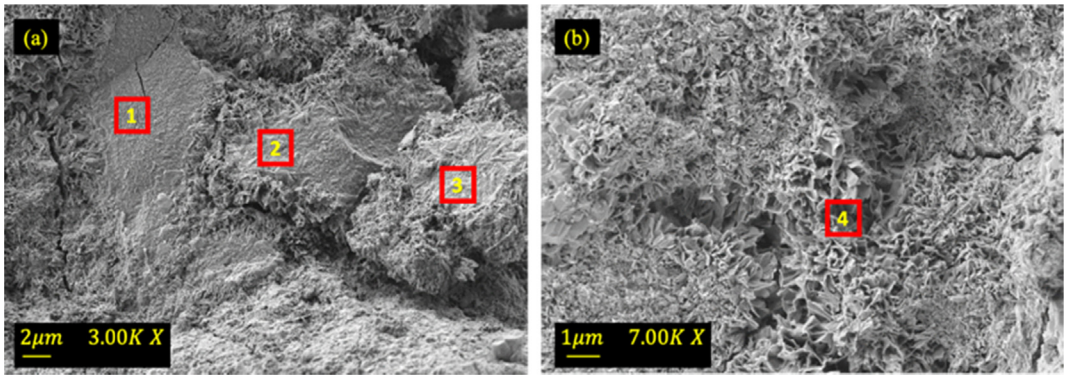

Fig. 11. FESEM micrographs for paste 4 mol KOH (7 curing days at 65 °C).

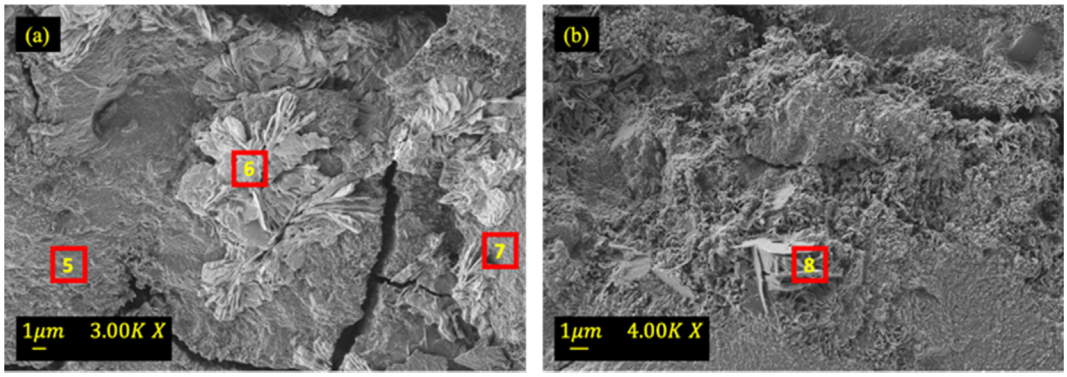

Fig. 12. FESEM micrographs for paste 8 mol KOH (7 curing days at 65 °C).

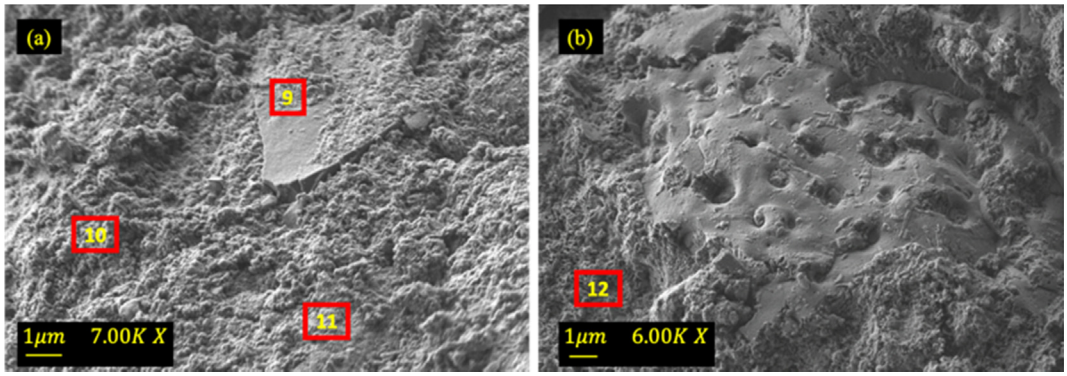

Fig. 13. FESEM micrographs for paste Rp20 (7 curing days at 65 °C).

XRD analysis and the thermal decomposition peaks obtained from the DTG curves were similar. However, for the Rp20 paste, the K_2O/BFS mass ratio was 0.117, and the XRD pattern and DTG curve were notably different. This mass ratio value was between the KOH-activated pastes, which suggests that not only the amount of potassium influence, but also the nature of the alkaline reagents present in ash (arkanite, fairchildite, bütschilite, and probably other amorphous K-containing phases), must be considered. Additionally, the presence of calcium compounds in ABA (e.g. calcite, portlandite, fairchildite, bütschilite, anhydrite) undoubtedly modified BFS alkali activation development. The joint presence in ash of both cations (potassium and calcium) probably favored the development of a new cementing gel, and, consequently, enhanced the mechanical properties found for the ABA-containing mortars.

Figs. 11–13 show some micrographs of the pastes cured for 7 days at 65 °C. Table 7 summarizes the chemical composition of the different spots taken by the EDS analysis. All the pastes had a compact microstructure with a different morphology to the cementing gels.

Fig. 11 shows two micrographs for the BFS activated with 4 mol of KOH. Four areas were selected to compare chemical compositions (see Table 7). The chemical composition calculated by the EDS analysis in spot 1 was similar to the composition summarized in Table 3 for BFS: this is a BFS particle that was partially reacted and covered by a small amount of cementing gel. Spots 2 and 3 had a similar composition and presented a significant percentage of potassium (K_2O = 16–19%). This means that the formed gel was a potassium-rich phase of type C(K)-A-S-H. More porous gel was also found in this paste (see Spot 4), for which the chemical composition slightly differed: in this case, the percentages of calcium and potassium were higher (20.06% K_2O; 40.97% CaO). There are compacted and porous gels to form the cementing matrix.

Fig. 12 shows the micrographs corresponding to the 8 mol KOH paste. Table 7 summarizes the chemical compositions for spots 5–8. There are different morphologies for the cementing gels, compacted and porous, but similarly to the 4 mol KOH paste. It is noticeable that the potassium content in the cementing gel was generally similar to or higher than that found for the 4 mol KOH paste, which agrees with the increased molality of the activating solution.

Finally, the products formed in the paste activated with ABA are shown in Fig. 13. In general, the cementing gels are more compacted than those found for the KOH-activated systems. The micrograph on the right (Fig. 13b) shows an unburned AS particle surrounded by cementing gel. On the one hand, regarding the chemical composition, potassium content was generally low, 10–13% K_2O (see spots 10–12), which means that, besides the proportion of K_2O for the Rp20 paste being between the 4 mol and 8 mol KOH pastes, less potassium was incorporated into the formed C(K)-A-S-H gel. Part of the potassium present in ABA was probably not dissolved during the reaction process. A similar result was obtained by de Moraes Pinheiro et al. [14] in their paper with the use of OBA as activator. On the other hand, the SiO_2 content was high (31–35%), which demonstrates the different nature of this cementing gel to those characterized by the KOH-activated pastes.

Table 7
Chemical composition by the EDS analysis for the pastes represented in Figs. 11–13.

Spot	Na_2O	MgO	Al_2O_3	SiO_2	SO_3	K_2O	CaO
1	–	12.88	14.27	30.98	1.87	3.95	36.04
2	–	18.38	13.59	27.39	2.13	18.79	19.72
3	0.58	17.19	13.11	26.86	1.19	16.88	24.20
4	0.90	2.04	8.01	24.04	3.49	20.06	40.97
5	–	–	1.98	17.27	2.25	32.28	45.61
6	–	1.39	2.42	12.75	2.47	48.55	32.42
7	0.55	16.23	10.15	22.52	2.18	21.32	27.05
8	1.29	–	10.79	29.66	1.45	17.45	39.34
9	–	7.91	9.61	31.10	–	21.96	25.92
10	0.76	4.80	9.34	32.26	–	10.90	41.94
11	–	12.54	13.87	32.13	1.95	10.99	28.53
12	–	6.63	10.77	35.07	1.87	12.87	32.79

3.4. Environmental aspects

Reusing waste such ABA, as a new raw material, is one of the main keys of circular economy. Commercial potassium hydroxide synthesis has a very high carbon footprint (1.649 $kgCO_2eq$/kg-KOH [43]). Despite the low quantity of KOH required to prepare the activating solutions in the control mortars, this component is the most important factor to take into account for these alkali-activated cement types. Furthermore, as BFS is considered a by-product of the iron industry, secondary production and the energy required for conditioning this precursor (drying, crushing) must be taken into account.

An environmental study was carried out to compare the manufacturing of 1 m^3 of the control mortars (4 mol and 8 mol), where KOH was employed for BFS activation. The Rp and Ad series mortars were selected, where ABA was employed for BFS activation. The selected mortars were: a) Rp20, Rp25 and Rp30 for the Rp series; b) Ad15, Ad20 and Ad25 for the Ad series. These selected systems yielded the best compressive strength development.

Table 8 summarizes the unitary results ($kgCO_2eq$) for the raw materials and activities (conditioning procedure) of the GWP100 calculations for 1 m^3 of each selected mortar.

Table 8
Unitary $kgCO_2eq$ for raw materials and conditioning procedure of the GWP100 calculations for 1 m^3 of each selected mortar.

	Components	Raw materials		Conditioning procedure (milling)	
		Unitary $kgCO_2eq$	Total $kgCO_2eq$	Unitary $kgCO_2eq$	Total $kgCO_2eq$
4 mol	BFS	9.1	82.7	43.2	43.2
	KOH	71.4		–	
	H_2O	0.1		–	
	Sand	2.1		–	
8 mol	BFS	9.2	191.8	43.7	43.7
	KOH	180.4		–	
	H_2O	0.1		–	
	Sand	2.1		–	
Rp20	BFS	7.5	9.7	35.3	41.2
	ABA	0.0		5.9	
	H_2O	0.1		–	
	Sand	2.1		–	
Rp25	BFS	7.3	9.5	34.3	41.5
	ABA	0.0		7.3	
	H_2O	0.1		–	
	Sand	2.2		–	
Rp30	BFS	6.6	8.8	31.1	39.3
	ABA	0.0		8.2	
	H_2O	0.1		–	
	Sand	2.1		–	
Ad15	BFS	9.3	11.5	44.0	47.6
	ABA	0.0		3.6	
	H_2O	0.1		–	
	Sand	2.1		–	
Ad20	BFS	9.0	11.2	42.5	47.4
	ABA	0.0		4.9	
	H_2O	0.1		–	
	Sand	2.1		–	
Ad25	BFS	8.8	10.9	41.5	47.4
	ABA	0.0		5.9	
	H_2O	0.1		–	
	Sand	2.0		–	

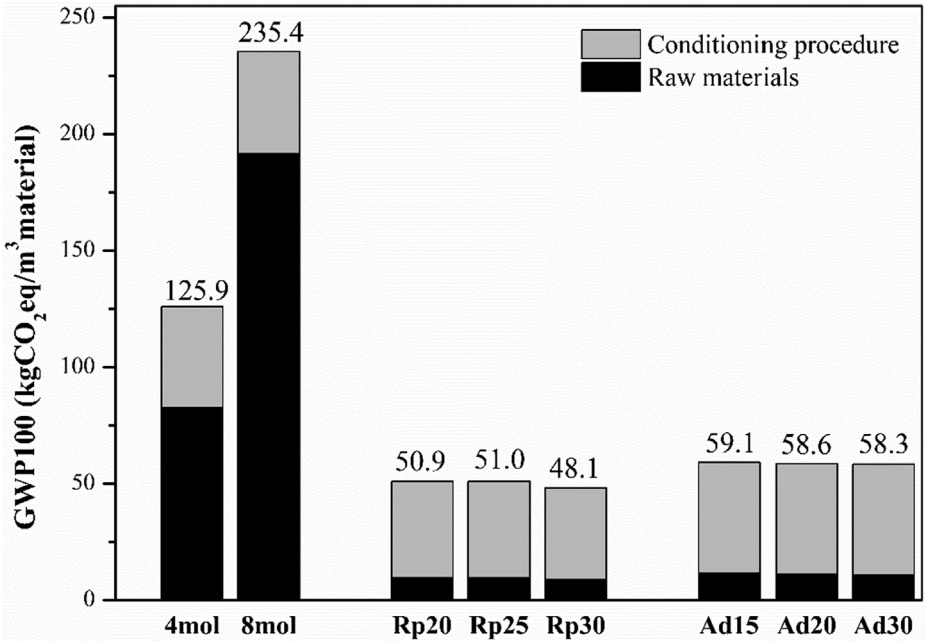

Fig. 14. GWP100 values for the control and selected ABA-containing mortars.

Water had the mildest influence in relation to the raw materials: around 0.1% for the control AAMs and 1% for the alternative AAMs. Furthermore, water did not influence materials conditioning.

In the prepared mortars, the sand:binder ratio came close to 3; that is, sand became the most representative component per mass in the dose of all the studied mortars (about 65–70%). However, its influence on CO_2 emissions was also weak compared to those for precursors or activators. For the 4 mol and 8 mol systems, sand represented 2.5% and 1.1% of emissions, respectively. In the alternative ABA-containing mortars (Rp and Ad series), the emissions related to sand lay between 20% and 25% of the emissions associated with raw materials. For all the studied mortars, the GWP100 of sand was around 2–2.2 $kgCO_2eq$. This component had no influence on the GWP100 calculations related to the conditioning procedures.

BFS was a by-product and its secondary production involved representative CO_2 emissions, which generally it means that about 6.6–9.2 $kgCO_2eq$ were emitted for 1 m^3 of mortar. An additional contribution to CO_2 emissions must be taken into account because it was necessary for conditioning (milling) to achieve enough fineness to be used as a precursor (31.1–43.7 $kgCO_2eq/m^3$ of mortar).

BFS presented a significant contribution to the CO_2 emissions for the control mortars (11.1% for 4 mol and 4.8% for 8 mol). However, their main influencing factor was the activator (KOH) despite it being the component used in the smallest quantity. This chemical reagent contributed 86% in 4 m and 94% in 8 m in associated emissions. BFS had a stronger influence as a raw material for the alternative ABA-containing mortars (around 75% in the Rp series and 80% in the Ad series).

Conversely, using ABA as a KOH replacement for BFS activation significantly reduced the emissions associated with obtaining raw materials. ABA is a waste material and not a by-product. On the negative side, it involves emissions associated with its required milling treatment. This means that for the total $kgCO_2eq/m^3$ associated with materials conditioning, the Ad series gave a slightly increase compared to 4 mol and 8 mol, but the Rp series involved fewer CO_2 emissions than the control ones. In any case, the reduction in GWP100 for the ABA-activated systems, compared to the 8 mol KOH sample, was very significant because the GWP100 value was 75–80% lower.

Finally, Fig. 14 compares the total GWP100 values. By doubling the molality (from 4 mol to 8 mol) in the control mortars, GWP100 increased by 87%.

A significant reduction took place with the alternative 100% waste-based AAM with ABA both for the Rp and Ad series. For them, the most important contribution was associated with the milling process.

These results offer a greener perspective in the construction material industry by means of circular economy implementation by using ABA as a new raw material. The environmental assessment demonstrated the potential reduction in GWP100 of these new ABA-activating mortars vs. traditional AAMs, for which a commercial chemical reagent (KOH) is necessary. This study was carried out with limited data on the raw material and its conditioning, but the following aspects should be considered in a real situation:

- The raw material milling was considered under laboratory conditions using a ball mill with a very limited capacity. An industrial mill should be employed for bigger volumes of materials, which would mean process optimization and thus a reduction in GPW100. the transport of raw materials from
- The extraction area to the manufacturing plant (the UPV laboratory in this case) was not considered in this “gate-to-gate” study. It is important to bear in mind the geographical location of waste and the volume of its production toward economically profitable implementation in manufacturing construction materials.

4. Conclusions

The ash obtained from AS combustion (ABA) was tested as an alkali activator in BFS-based activated cement. The potassium salts present in ABA promoted BFS hydraulicity. The cementing gel of type C(K)-A-S-H was produced by mixing ABA, BFS and water, with curing at 65 °C for 3 and 7 days. These gels yielded a good strength development of the ABA/BFS mortars, with compressive strength

values within the 25–45 MPa range after 7 curing days at 65 °C. These values were higher than those obtained using KOH solutions (molalities: 4 mol and 8 mol). The best BFS/ABA mass ratio fell with the 2–7 range. For the Rp series (ABA replaced BFS) and the Ad series (ABA was added to a constant amount of BFS), the best result was obtained for 25%. The CO_2 emissions associated with the BFS-activated cement reduced when ABA was used as a chemical activator compared to the KOH activator. In this way, the ABA containing binder comes over as a greener option (around 75–80% reduction in CO_2) and contributes to circular economy.

Declaration of Competing Interest

There are no conflicts to declare.

Acknowledgements

We wish to thank the Spanish Government for project support (MINECO/FEDER-Project RTI2018-09612-B-C21). The authors would like to thank Borges Agricultural & Industrial Nuts for supplying the biomass ash and the Electronic Microscopy Service at the UPV.

References

[1] A. Hassan, M. Arif, M. Shariq, Use of geopolymer concrete for a cleaner and sustainable environment – a review of mechanical properties and microstructure, J. Cleaner Prod. 223 (2019) 704–728, https://doi.org/10.1016/j.jclepro.2019.03.051.
[2] F. Pacheco-Torgal, J.A. Labrincha, C. Leonelli, A. Palomo, P. Chindaprasirt, Handbook of Alkali-activated Cements, Mortars and Concretes. Woofgead Publish, 2015., Woodhead Publishing, 2015. DOI:10.1016/C2013-0-16511-7.
[3] A. Palomo, P. Krivenko, I. Garcia-Lodeiro, E. Kavalerova, O. Maltseva, A. Fernández-Jiménez, A review on alkaline activation: new analytical perspectives, Materiales de Construccion. 64 (315) (2014) e022, https://doi.org/10.3989/mc.2014.00314.
[4] E. Altan, S.T. Erdoğan, Alkali activation of a slag at ambient and elevated temperatures, Cem. Concr. Compos. 34 (2012) 131–139, https://doi.org/10.1016/j.cemconcomp.2011.08.003.
[5] O.A. Mohamed, A review of durability and strength characteristics of alkali-activated slag concrete, Materials 12 (2019) 1198, https://doi.org/10.3390/ma12081198.
[6] T. Bakharev, J.G. Sanjayan, Y.-B. Cheng, Effect of admixtures on properties of alkali-activated slag concrete, Cem. Concr. Res. 30 (2000) 1367–1374, https://doi.org/10.1016/S0008-8846(00)00349-5.
[7] E. Jamieson, C.S. Kealley, A. Van Riessen, R.D. Hart, Optimising ambient setting Bayer derived fly ash geopolymers, Materials 9 (2016) 19–22, https://doi.org/10.3390/ma9050392.
[8] A. Fernández-Jiménez, N. Cristelo, T. Miranda, Á. Palomo, Sustainable alkali activated materials: precursor and activator derived from industrial wastes, J. Cleaner Prod. 162 (2017) 1200–1209, https://doi.org/10.1016/j.jclepro.2017.06.151.
[9] J.M. Mejía, R. Mejía de Gutiérrez, F. Puertas, Ceniza de cascarilla de arroz como fuente de sílice en sistemas cementicios de ceniza volante y escoria activados alcalinamente, Materiales de Construccion. 63 (2013) 361–375, https://doi.org/10.3989/mc.2013.04712.
[10] J.C.B. Moraes, A. Font, L. Soriano, J.L. Akasaki, M.M. Tashima, J. Monzó, M.V. Borrachero, J. Payá, New use of sugar cane straw ash in alkali-activated materials: a silica source for the preparation of the alkaline activator, Constr. Build. Mater. 171 (2018) 611–621, https://doi.org/10.1016/j.conbuildmat.2018.03.230.
[11] A. Mellado, C. Catalán, N. Bouzón, M.V. Borrachero, J.M. Monzó, J. Payá, Carbon footprint of geopolymeric mortar: study of the contribution of the alkaline activating solution and assessment of an alternative route, RSC Adv. 4 (2014) 23846–23852, https://doi.org/10.1039/C4RA03375B.
[12] A. Peys, H. Rahier, Y. Pontikes, Potassium-rich biomass ashes as activators in metakaolin-based inorganic polymers, Appl. Clay Sci. 119 (2016) 401–409, https://doi.org/10.1016/j.clay.2015.11.003.
[13] A. Font, L. Soriano, J.C.B. Moraes, M.M. Tashima, J. Monzó, M.V. Borrachero, J. Payá, A 100% waste-based alkali-activated material by using olive-stone biomass ash (OBA) and blast furnace slag (BFS), Mater. Lett. 203 (2017) 46–49, https://doi.org/10.1016/j.matlet.2017.05.129.
[14] S.M. de Moraes Pinheiro, A. Font, L. Soriano, M.M. Tashima, J. Monzó, M.V. Borrachero, J. Payá, Olive-stone biomass ash (OBA): an alternative alkaline source for the blast furnace slag activation, Constr. Build. Mater. 178 (2018) 327–338, https://doi.org/10.1016/j.conbuildmat.2018.05.157.
[15] M.M. Alonso, C. Gascó, M.M. Morales, J.A. Suárez-Navarro, M. Zamorano, F. Puertas, Olive biomass ash as an alternative activator in geopolymer formation: a study of strength, durability, radiology and leaching behaviour, Cem. Concr. Compos. 104 (2019), https://doi.org/10.1016/j.cemconcomp.2019.103384 103384.
[16] A. Font, L. Soriano, S.M. de Moraes Pinheiro, M.M. Tashima, J. Monzó, M.V. Borrachero, J. Payá, Design and properties of 100% waste-based ternary alkali-activated mortars: blast furnace slag, olive-stone biomass ash and rice husk ash, J. Cleaner Prod. 243 (2020) 118568, https://doi.org/10.1016/j.jclepro.2019.118568.
[17] W.Y. Lin, A.K. Prabhakar, B.C. Mohan, C.-H. Wang, A factorial experimental analysis of using wood fly ash as an alkaline activator along with coal fly ash for production of geopolymer-cementitious hybrids, Sci. Total Environ. 718 (2020) 135289, https://doi.org/10.1016/j.scitotenv.2019.135289.
[18] S.V. Vassilev, D. Baxter, L.K. Andersen, C.G. Vassileva, An overview of the chemical composition of biomass, Fuel 89 (2010) 913–933, https://doi.org/10.1016/j.fuel.2009.10.022.
[19] Consejería de Agricultura Pesca y Desarollo Rural, Caracterización del sector de la almendra en Andalucía, (2016) 1–34.
[20] Statista GmbH, Tree nuts: world markets and trade. USDA. United States Department of Agriculture Service. Foreign Agricultural Service, (n.d.). https://www.statista.com/ (accessed May 10, 2020).
[21] A. Benítez, M. González-Tejero, Á. Caballero, J. Morales, Almond shell as a microporous carbon source for sustainable cathodes in lithium-sulfur batteries, Materials 11 (2018) 1428, https://doi.org/10.3390/ma11081428.
[22] C.S.G.P. Queirós, S. Cardoso, A. Lourenço, J. Ferreira, I. Miranda, M.J.V. Lourenço, H. Pereira, Characterization of walnut, almond, and pine nut shells regarding chemical composition and extract composition, Biomass Convers. Biorefin. 10 (2020) 175–188, https://doi.org/10.1007/s13399-019-00424-2.
[23] N. Europea, N. Une-en, Biocombustibles sólidos. Especificaciones y clases de combustibles. Parte 1: Requisitos generales, (2014).
[24] M.G. Pinna-Hernández, I. Martínez-Soler, M.J. Díaz Villanueva, F.G. Acien Fernández, J.L.C. López, Selection of biomass supply for a gasification process in a solar thermal hybrid plant for the production of electricity, Ind. Crops Prod. 137 (2019) 339–346, https://doi.org/10.1016/j.indcrop.2019.04.060.
[25] R. García, C. Pizarro, A.G. Lavín, J.L. Bueno, Biomass sources for thermal conversion. Techno-economical overview, Fuel 195 (2017) 182–189, https://doi.org/10.1016/j.fuel.2017.01.063.
[26] T. Aktas, P. Thy, R.B. Williams, Z. McCaffrey, R. Khatami, B.M. Jenkins, Characterization of almond processing residues from the Central Valley of California for thermal conversion, Fuel Process. Technol. 140 (2015) 132–147, https://doi.org/10.1016/j.fuproc.2015.08.030.
[27] C.D. Blasi, A. Galgano, C. Branca, Exothermic events of nut shell and fruit stone pyrolysis, ACS Sustainable Chem. Eng. 7 (2019) 9035–9049, https://doi.org/10.1021/acssuschemeng.9b01474.
[28] AENOR, UNE-EN 196-1, Methods of Testing Cement – Part 1: Determination of Strength, (2005).
[29] S. Eggleston, L. Buendia, K. Miwa, T. Ngara, K. Tanabe, Foreword Preface 2006 IPCC Guidelines for National Greenhouse Gas Inventories, 2006 IPCC Guidelines for National Greenhouse Gas Inventories. (2006) 6. http://www.ipcc-nggip.iges.or.jp/public/2006gl/pdf/0_Overview/V0_0_Cover.pdf.
[30] CNMC, Sede electrónica - Listado de Informes de Etiquetado de Electricidad, Comisión Nacional de Los Mercados y La Competencia. (2018). https://gdo.cnmc.es/CNE/resumenGdo.do?anio=2018 (accessed August 21, 2019).
[31] Eric D. Vance, Land application of wood-fired and combination boiler ashes: an overview, J. Environ. Qual. 25 (1996) 937–944, https://doi.org/10.2134/jeq1996.00472425002500050002x.
[32] Ayhan Demirbaş, Fuel characteristics of olive husk and walnut, hazelnut, sunflower, and almond shells, Energy Sources 24 (2002) 215–221, https://doi.org/10.1080/009083102317243601.
[33] B.K. Shah, C.G. Khatri, A method of fitting the regression curve E(y) = α + δx + βρx, Technometrics 7 (1965) 59–65, https://doi.org/10.1080/00401706.1965.10490226.
[34] Stanislav V. Vassilev, Christina G. Vassileva, Water-soluble fractions of biomass and biomass ash and their significance for biofuel application, Energy Fuels 33 (2019) 2763–2777, https://doi.org/10.1021/acs.energyfuels.9b00081.
[35] Cengiz Duran Atiş, Cahit Bilim, Özlem Çelik, Okan Karahan, Influence of activator on the strength and drying shrinkage of alkali-activated slag mortar, Constr. Build. Mater. 23 (2009) 548–555, https://doi.org/10.1016/j.conbuildmat.2007.10.011.
[36] A.F. Abdalqader, F. Jin, A. Al-Tabbaa, Development of greener alkali-activated cement: utilisation of sodium carbonate for activating slag and fly ash mixtures, J. Cleaner Prod. 113 (2016) 66–75, https://doi.org/10.1016/j.jclepro.2015.12.010.
[37] H.A. Abdel-Gawwad, S. Abd El-Aleem, Effect of reactive magnesium oxide on properties of alkali activated slag geopolymer cement pastes, Ceramics - Silikaty. 59 (2015) 37–47. https://www.scopus.com/inward/record.uri?eid=2-s2.0-84938304796&partnerID=40&md5=e5f33ef4d02081a175afed69f3d0943f.

[38] R.M. Queiroz, Luiza H.O. Pires, Ruth C.P. de Souza, J.R. Zamian, A.G. de Souza, G. N. da Rocha Filho, C.E.F. da Costa, Thermal characterization of hydrotalcite used in the transesterification of soybean oil, J. Therm. Anal. Calorim. 97 (2009) 163–166, https://doi.org/10.1007/s10973-009-0246-6.
[39] A.M. Humad, K. Habermehl-Cwirzen, A. Cwirzen, Effects of fineness and chemical composition of blast furnace slag on properties of Alkali-Activated Binder, Materials 12 (2019) 1–17, https://doi.org/10.3390/ma12203447.
[40] E. Bonaccorsi, S. Merlino, A.R. Kampf, The crystal structure of tobermorite 14 Å (plombierite), a C-S-H phase, J. Am. Ceram. Soc. 88 (2005) 505–512, https://doi.org/10.1111/j.1551-2916.2005.00116.x.
[41] Z. Shi, C. Shi, S. Wan, N. Li, Z. Zhang, Effect of alkali dosage and silicate modulus on carbonation of alkali-activated slag mortars, Cem. Concr. Res. 113 (2018) 55–64, https://doi.org/10.1016/j.cemconres.2018.07.005.
[42] Hailong Ye, Chuanqing Fu, Guojun Yang, Alkali-activated slag substituted by metakaolin and dolomite at 20 and 50°C, Cem. Concr. Compos. 105 (2020) 103442, https://doi.org/10.1016/j.cemconcomp.2019.103442.
[43] OpenLCA.org, ecoinvent 3.3 released in openLCA Nexus databases, (n.d.). https://www.openlca.org/ecoinvent-3-3-released-in-openlca-nexus/ (accessed May 10, 2020).